ACS APPLIED MATERIALS & INTERFACES

Research Article

Cite This: ACS Appl. Mater. Interfaces 2018, 10, 38264−38271

www.acsami.org

Consecutive Junction-Induced Efficient Charge Separation Mechanisms for High-Performance MoS_2/Quantum Dot Phototransistors

Sangyeon Pak,[†,∇] Yuljae Cho,[†,∇] John Hong,[†] Juwon Lee,[†] Sanghyo Lee,[†] Bo Hou,[†] Geon-Hyoung An,[†] Young-Woo Lee,[‡] Jae Eun Jang,[§] Hyunsik Im,[∥] Stephen M. Morris,[†] Jung Inn Sohn,[*,∥] SeungNam Cha,[*,†,⊥] and Jong Min Kim[#]

[†]Department of Engineering Science, University of Oxford, Parks Road, Oxford OX1 3PJ, United Kingdom

[‡]Department of Energy Systems, Soonchunhyang University, Asan31538, Chungcheongnam-do, Republic of Korea

[§]Department of Information and Communication Engineering, Daegu Gyeongbuk Institute of Science and Technology (DGIST), Daegu 711-873, Republic of Korea

[∥]Division of Physics and Semiconductor Science, Dongguk University, Seoul 04620, Republic of Korea

[⊥]Department of Physics, Sungkyunkwan University, Suwon 16419, Gyeonggi-do, Republic of Korea

[#]Electrical Engineering Division, Department of Engineering, University of Cambridge, 9 JJ Thomson Avenue, Cambridge CB3 0FA, United Kingdom

Supporting Information

ABSTRACT: Phototransistors that are based on a hybrid vertical heterojunction structure of two-dimensional (2D)/quantum dots (QDs) have recently attracted attention as a promising device architecture for enhancing the quantum efficiency of photodetectors. However, to optimize the device structure to allow for more efficient charge separation and transfer to the electrodes, a better understanding of the photophysical mechanisms that take place in these architectures is required. Here, we employ a novel concept involving the modulation of the built-in potential within the QD layers for creating a new hybrid MoS_2/PbS QDs phototransistor with consecutive type II junctions. The effects of the built-in potential across the depletion region near the type II junction interface in the QD layers are found to improve the photoresponse as well as decrease the response times to 950 μs, which is the faster response time (by orders of magnitude) than that recorded for previously reported 2D/QD phototransistors. Also, by implementing an electric-field modulation of the MoS_2 channel, our experimental results reveal that the detectivity can be as large as 1×10^{11} jones. This work demonstrates an important pathway toward designing hybrid phototransistors and mixed-dimensional van der Waals heterostructures.

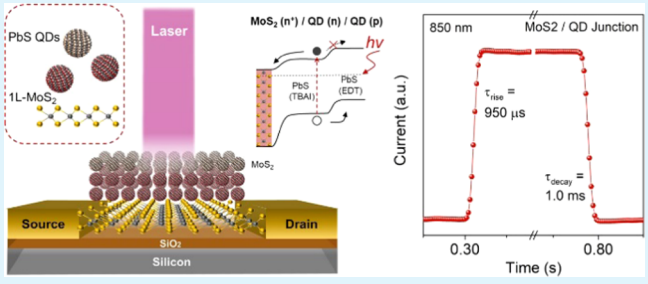

KEYWORDS: *molybdenum disulfide, lead sulfide quantum dots, hybrid phototransistors, built-in potential, fast photodetectors*

INTRODUCTION

Photodetectors that convert photonic energy into electrical signals have been key building blocks for devices in modern communication and imaging applications, and their compatibility with complementary metal−oxide−semiconductor technology has enabled extensive and widespread utilization.[1] Of increasing technological importance for next-generation, high-performance, and flexible/wearable photosensing applications is the need to develop new nanostructured materials that have distinct properties from their conventional bulk counterparts and an understanding of the various physical phenomena that are observed in these new device architectures so that the performance of the optoelectronic devices can be maximized.[2−4] In this sense, photodetectors based on low-dimensional materials such as quantum dots (QDs),[5−9] nanowires,[10,11] graphene,[12] and monolayer transition metal dichalcogenides[3,13,14] have been developed, as they possess unique and unconventional properties such as strong light−matter interaction, tunable optical absorption, outstanding carrier transport, and so on, leading to an enormous variety of possibilities in optoelectronic performance and functionality.

To enhance the performance of photodetectors based on low-dimensional materials, phototransistors with a vertical heterojunction structure have very recently attracted significant

Received: August 21, 2018
Accepted: October 8, 2018
Published: October 19, 2018

DOI: 10.1021/acsami.8b14408
ACS Appl. Mater. Interfaces 2018, 10, 38264−38271

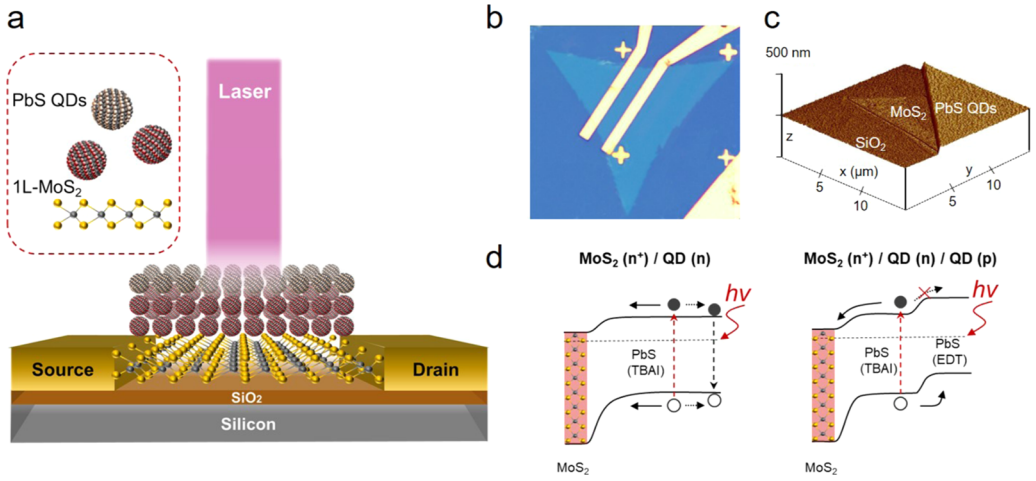

Figure 1. MoS_2/PbS QD hybrid structure design and architecture. (a) An illustration of our hybrid-structured phototransistor. The illustration of the monolayer MoS_2 and PbS QDs are enlarged in the inset. (b) Optical microscopy image of the MoS_2 device fabricated using electron-beam lithography. (c) Three-dimensional atomic force microscopy image of the MoS_2/PbS QDs hybrid structure. (d) Illustration of the band alignments of the MoS_2/PbS−TBAI and MoS_2/PbS−TBAI/PbS−EDT structures. Note that the large built-in potential is created within the QD layers for the MoS_2/PbS−TBAI/PbS−EDT device.

attention, as they can improve the quantum efficiency of the detector. The improvement is attributed to the design of the phototransistor structure utilizing the high mobility of the channel materials, which results in fast charge carrier transport coupled with the strong light-absorbing semiconductors that are coated onto the channel leads to a favorable alignment of the energy bands ensuring efficient charge transfer.[15,16] With the advent of two-dimensional (2D) materials such as graphene and MoS_2, phototransistor architectures that combine a 2D material channel with semiconducting nanoparticles have achieved unprecedented sensitivity and gain.[17] The recent development of this hybrid architecture has already been shown to be compatible with a variety of 2D materials and colloidal quantum dots.[15,18−21] Furthermore, the 2D/QD combination has been recognized as a particularly desirable structure, associated with thin, transparent, and high mobility of the 2D structures and the extra degree of freedom in terms of the location of the absorption spectrum, which arises from the tunability of the optical band gap of QDs. Nevertheless, the light-absorbing medium needs to transport photogenerated carriers more quickly and efficiently in a preferential direction, otherwise it can limit the overall external quantum efficiency and response time of the detector.[19] For 2D/QD phototransistors with a vertical heterojunction platform, a built-in potential is created at the 2D channel and the QD interface only. Therefore, the overall performance of the hybrid structure photodetector is limited by the energy band alignment of the QD layers that govern the dissociation of the photogenerated excitons and the diffusion of the charge carriers within the thick QD layers. As a result, an additional driving force is required in the heterojunction device to facilitate improved exciton dissociation and charge transfer within the light-absorbing QD layer to effectively inject photogenerated carriers into the channel.

Herein, we employ a novel concept involving the modulation of a built-in potential within the QD layers. A consecutive type II junction structure is formed that effectively dissociates and transfers photogenerated carriers to the channel, which enhances the overall optoelectronic performance of the phototransistor that has a vertical heterojunction structure. We employed prevalent colloidal lead sulfide (PbS) QDs and an MoS_2 2D structure to demonstrate the performance of the conceptual phototransistor design. The built-in potential was created by surface modification to the PbS QD layers sequentially using n-type tetrabutylammonium iodide (TBAI) and p-type 1,2-ethanedithiol (EDT) ligands, which is a well-known surface engineering strategy to create p−n junctions in PbS QDs photovoltaics.[22] Also, a monolayer of MoS_2 was employed as the channel material, as it can effectively transport photogenerated carriers through the field-effect control of the conductivities. The efficient separation of charge carriers that results from the electric field created by the built-in potential in the QD layers is found to lead to an increase in the photocurrent as well as the photoresponsivity. Further, we observe an improvement in the response time to values below 1 ms when the built-in potential is employed in the QD layers and attribute the reduced time to an enhanced charge transfer as a result of the drift of electrons within the QD layers. This response time is the fastest time reported thus far for a 2D/QD hybrid phototransistor. By applying a gate electric field to the channel, the detectivity of the junction-controlled device could be increased to values up to 10^{11} jones. This proof-of-concept device represents an important strategy toward designing mixed-dimensional van der Waals heterostructures.

RESULTS AND DISCUSSION

The hybrid MoS_2/PbS QDs phototransistor device architecture is illustrated in Figure 1a. A monolayer of MoS_2 was synthesized on a 300 nm SiO_2/Si substrate using a chemical vapor deposition (CVD) method, and the crystal quality of the MoS_2 layer was confirmed using Raman spectroscopy, photoluminescence (PL) spectroscopy, and transmission electron microscopy (TEM) measurements (Figures S1 and S2). The fabrication of the hybrid-structured device began by patterning the source−drain electrodes using e-beam lithography, followed by the thermal deposition of (5/45 nm) Ti/Au layers (Figure 1b). We then spin-coated six layers of PbS QDs onto the device by employing a layer-by-layer process (Figure S3). The thickness was chosen to achieve optimized perform-

DOI: 10.1021/acsami.8b14408
ACS Appl. Mater. Interfaces 2018, 10, 38264−38271

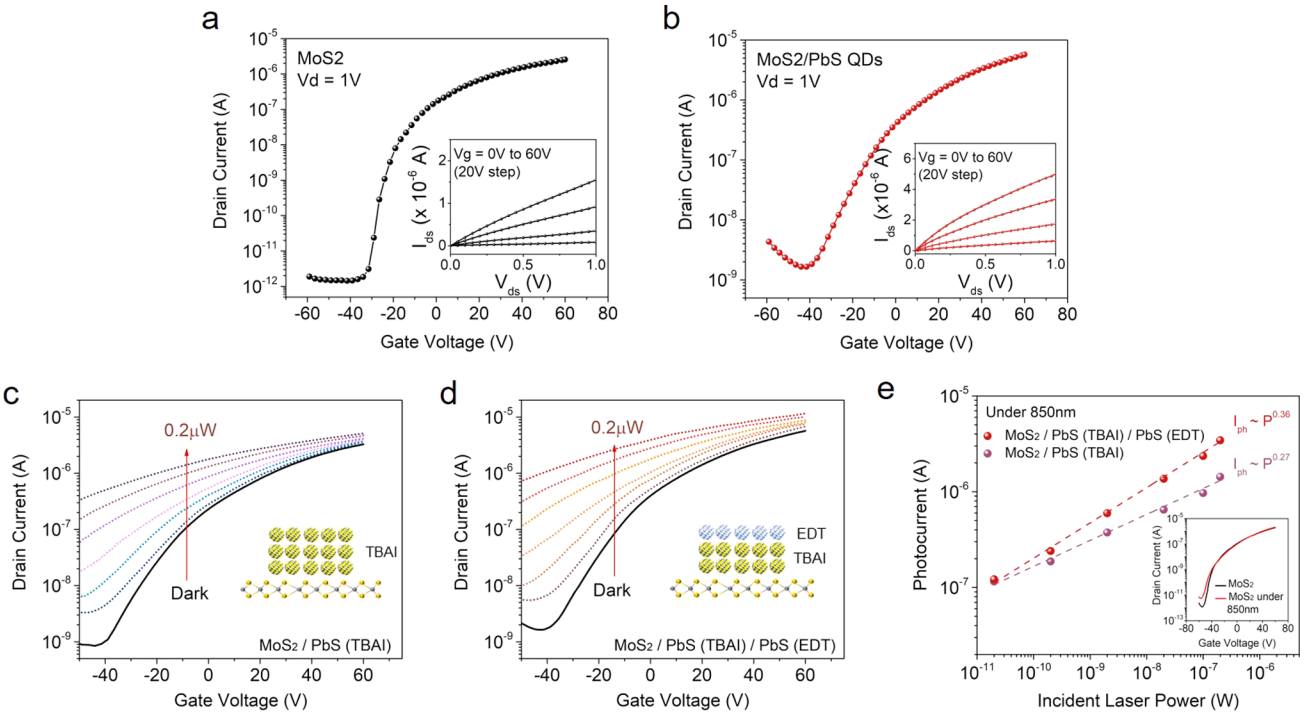

Figure 2. Electrical and photoelectrical measurements of the MoS_2/PbS hybrid-structured device under 850 nm laser excitation. Transfer curves of (a) the pristine MoS_2 and (b) MoS_2/PbS devices. The transfer curves were measured for a drain voltage of V_d = 1 V in ambient and dark conditions. The inset images show the output curves of the respective devices. (c, d) Measurements of the drain current as a function of gate voltage for the MoS_2/TBAI and MoS_2/TBAI/EDT devices when illuminated with an 850 nm laser at different incident intensities (dark—200 nW). (e) Photocurrent as a function of the incident laser power for the MoS_2/TBAI and MoS_2/TBAI/EDT devices. The exponent in the power-law dependence of the photocurrent generation with incident laser power was found to increase from 0.27 to 0.36 when an internal electric field in the QD layers was employed.

ance by taking into account the diffusion length of the PbS QDs, which is reported elsewhere.[19,21,23] Figure 1c shows a three-dimensional atomic force microscopy (AFM) image of edge of the MoS_2 and PbS QDs on the SiO_2 substrate so as to clearly illustrate our hybrid-structured device. The resulting electrical properties of the MoS_2 and hybrid-structured devices are analyzed in Figure 2a,b. The pristine MoS_2 device showed excellent gate-modulated current with an on/off ratio greater than 10^6 and a calculated mobility of 3 $cm^2/(V\ s)$, whereas the PbS QD-deposited MoS_2 device exhibited a slightly higher current with an increased mobility of 3.4 $cm^2/(V\ s)$, possibly due to the transfer of charges from the PbS QD layers to the MoS_2 monolayer associated with a type II heterojunction.[20]

MoS_2/QD Phototransistor Device Design. The basic principle of the device design and operation is captured in the band alignment of the MoS_2 channel and the light-absorbing PbS QDs as shown in Figure 1d. We have designed a p−n junction structure into the PbS QD layers and have compared the performance of the device with the one that does not have any form of junction in the QD layers, so as to verify the effectiveness of the built-in potential in the QD layers. The two device architectures are phototransistors with (1) MoS_2 and TBAI-treated PbS QDs (TBAI−PbS) and (2) MoS_2, TBAI−PbS, and EDT-treated PbS QDs (EDT−PbS). In the first device architecture (Figure 1d, left), the built-in potential is created only at the interface between the MoS_2 and TBAI−PbS layers, arising from the formation of a type II heterojunction. Similarly, the second device architecture (Figure 1d, right) has the same built-in potential at the interface; however, another large built-in potential is formed within the QD layers when the energy bands of the n-type TBAI−PbS and the p-type EDT−PbS layers are aligned. Note that the thickness of QD layers and the MoS_2/TBAI−PbS interface are identical in both cases to rule out any unintended mismatches in the two device architectures. Also, the same thickness of QD layers in both devices guarantees that light absorption is equivalent. Colloidal PbS QDs (PbS CQDs) with a band gap energy of 1.3 eV (Figures S4 and S5) are employed in these devices. This particular QD size has been reported to efficiently absorb the incident and the surface properties can be readily modified with the addition of TBAI and EDT ligands (Figure S6).[22] To confirm the energy band alignment of the surface-treated PbS QDs, we investigated the energy band levels using ultraviolet photoelectron spectroscopy (UPS) (Figure S7). The measured and calculated energy levels of the TBAI−PbS and EDT−PbS layers confirm a large built-in potential of 0.31 eV when the energy bands are aligned, and the determined energy band alignment and offset value lead to the formation of a depletion region adjacent to the interface of TBAI−PbS and EDT−PbS layers, which effectively extends the depletion region throughout the QD layers. Therefore, the MoS_2/TBAI−PbS/EDT−PbS configuration can be understood as having an n^+−n−p architecture (double junction) with a depletion region at the TBAI−PbS/EDT−PbS interface, whereas the MoS_2/TBAI−PbS configuration can be considered as having an n^+−n architecture (single junction) in which the majority of the QD volume remains as a quasi-neutral region. It is worth mentioning that the large built-in potential (0.31 eV), which is sufficiently larger than the exciton binding energy of PbS QDs (~100 meV),[24,25] in the QD layers is expected to facilitate

DOI: 10.1021/acsami.8b14408
ACS Appl. Mater. Interfaces 2018, 10, 38264−38271

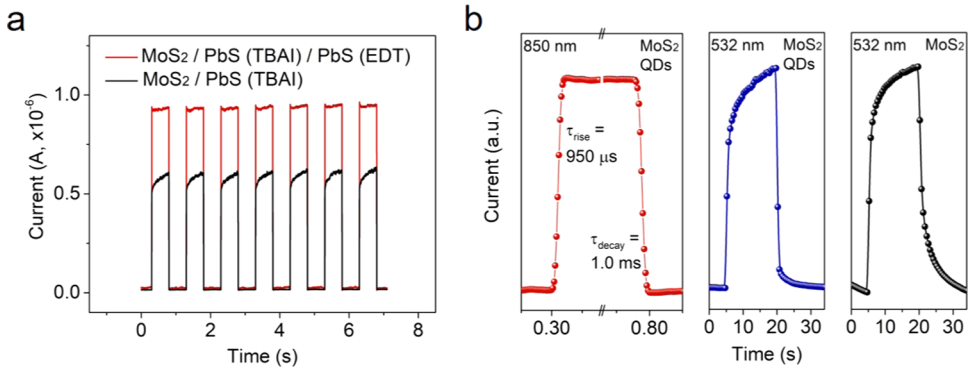

Figure 3. Photoresponse of the MoS_2/PbS QDs devices. (a) Temporal response of the photocurrent in the MoS_2/TBAI and MoS_2/TBAI/EDT devices under 850 nm laser illumination with V_d = 1 V, V_g = 0 V, P_{laser} = 200 nW. (b) Temporal response of the photocurrent showing a distinctly different response time when the incident energy (850 or 532 nm) is either smaller or larger than the band gap of the MoS_2 monolayer.

exciton dissociation[19] as well as the transfer of photogenerated electrons in a preferential direction from the QD layers toward the MoS_2 channel with the assistance of an internal electric field.

Enhancement in Photocurrent Collection. To prove that there is an enhancement in the charge collection efficiency in our junction-controlled device, we have measured the drain−source current, I_{ds}, as a function of the gate voltage, V_g, under various illumination intensities. Here, an 850 nm wavelength laser is used so that absorption only occurs in the QD layers and so that the transfer of photogenerated carriers can be carefully examined. The total incident laser power on the effective area is estimated by considering the laser spot size (diameter 500 μm) and the device active area (200 μm^2). As shown in Figure 2c,d, the photocurrent $I_{Ph} = I_{illumination} - I_{dark}$ of the double-junction device is higher than that of the single-junction device at the same V_g, V_{ds}, and incident laser power. To compare the different band alignments for the two device architectures, the power density dependence of the photocurrent of the devices was compared at V_g = 0 V (Figure 2e). In this case, the monolayer of MoS_2 (E_g = 1.88 eV) does not respond to the 850 nm laser as shown in the inset of Figure 2e. This is because the energy of the 850 nm laser is below the band gap of MoS_2 monolayer, and, therefore, the photocurrent generation takes place exclusively in the QD layers so that the two device architectures can be reasonably compared. At a gate voltage of V_g = 0 V, the photocurrent of the hybrid structure devices increases sublinearly with incident laser power ($I_{Ph} \approx P^{\alpha}$, $\alpha < 1$). However, this dependence is clearly increased for the double-junction device when compared to the single-junction device, with the exponent α increasing from 0.27 to 0.36. The increase in the photocurrent as well as the value of the exponent implies that more photogenerated electrons are transferred to the MoS_2 and the loss of photogenerated carriers through recombination is reduced, and is believed to be due to the formation of an internal electric field in the photoactive QD layers.[19]

Based on the photocurrent measurements for the hybrid-structured devices, the photoresponsivity and photogain can be evaluated. Photoresponsivity (R) of a phototransistor is estimated using the equation $R = I_{Ph}/P$, where P is the incident laser power on an effective area of the device. At an incident laser power of P = 2 nW, V_g = 0 V, and V_{ds} = 1 V, the photoresponsivity is calculated to be R = 187.1 A/W for the single-junction device. However, the photoresponsivity is increased to R = 297.5 A/W for the double-junction device under the same conditions. When the incident laser power is substantially reduced to P = 20 pW, R is found to be 5700 ± 71.2 and 6120 ± 96.9 A/W for the single-junction and double-junction devices, respectively (Figure S8). It is observed that the effect of built-in potential was more noticeable under the higher illumination intensities compared to the lower illumination intensities possibly due to the reduced recombination of carriers that can be particularly dominant for high carrier densities.[26]

The large photoresponsivity in our hybrid-structured devices benefits from the existence of the type II heterojunction that is formed between the channel and the light-absorbing medium, where photoinduced excitons are spatially separated, resulting in an extended lifetime; upon illumination, photogenerated electrons are transferred and circulated in the monolayer MoS_2 and photogenerated holes are trapped in the QD layers, resulting in a photoconductive gain. This gain[21,27] can be estimated using $G = \frac{\tau_{life}}{\tau_{transit}}$, where the value τ_{life} = 1 ms can be extracted from the temporal response of the hybrid-structured device (Figure 3) and carrier transit time $\tau_{transit}$ can be estimated using $\tau_{transit} = \frac{L^2}{\mu V_{ds}} = 83$ ns, where L is the channel length, μ is the field-effect mobility of MoS_2, and V_{ds} is the applied drain−source voltage. The carrier transit time is found to be orders of magnitude shorter than the lifetime of the carriers trapped in the QD layers. Therefore, electrons can be recirculated to achieve a photoconductive gain higher than 10^5.

Improved Photoresponse Time through Built-in Potential. We now turn our focus to the effect of the built-in potential that exists in the QD layers on the photoresponse time. The electric field (E) created by the built-in potential in the QD layers is expected to aid the effective separation of exciton pairs and increase the transit time of free carriers in the QD layers. Figure 3a shows the stable and repeated temporal response of our hybrid-structured devices after switching the 850 nm laser illumination on and off for 1 s under bias voltages of V_{ds} = 1 V and V_g = 0 V. For comparison, the behavior of a single-junction device is also presented. From the graph, we can clearly observe that the on-current level and rise times are different for the two devices. As demonstrated in Figure 2, the double-junction device shows a higher photocurrent level (increased by 50%) compared to the single-junction device. An interesting phenomenon is also shown during the off-to-on process, where we have measured the rise time (10 to 90% of

DOI: 10.1021/acsami.8b14408
ACS Appl. Mater. Interfaces 2018, 10, 38264−38271

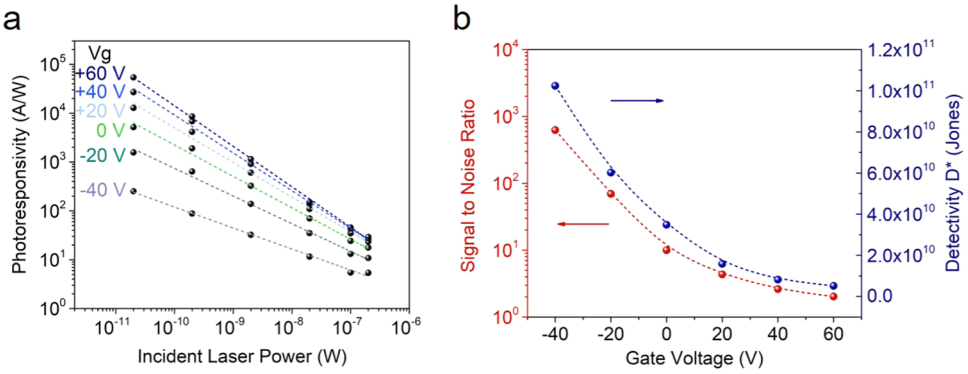

Figure 4. Phototransistor performance of the MoS_2/TBAI/EDT device for different applied gate voltages. (a) Photoresponsivity as a function of different back-gate voltages with a 1 V drain voltage and 850 nm laser illumination. (b) Signal-to-noise (SNR) ratio and measured detectivity D^* as a function of the back-gate voltages. An optimum detectivity of more than $D^* = 1 \times 10^{11}$ jones was obtained when the device was operated with a negative polarity gate bias voltage.

the dark to on-level). For the single-junction device, the photocurrent rise times are relatively slow (40 ms), whereas for the double-junction device, the current rises quickly (950 μs) and sharply before reaching a constant value.

The dramatic 42-fold improvement in the rise time can be attributed to the drift of dissociated excitons in the depletion region formed within the QD layers. In the depletion region of the QD layers, carriers are swept out in the form of drift current, leading to the initially rapid rise time of the photocurrent.[28,29] The rise time that is enhanced by the formation of the junction is strongly dependent on the depletion region transit time $\left(\tau_{\mathrm{Tr,depletion}} = \frac{W_{\mathrm{depletion}}}{\mu_{\mathrm{drift}} E}\right)$, where $W_{\mathrm{depletion}}$ is the depletion width, μ_{drift} is the drift mobility, and E is the internal electric field created at the QD junction. Therefore, it can be seen that the transport of photogenerated charge carriers within the QD layers is dominated by the drift, rather than the diffusion, due to the reduced quasi-neutral region wider depletion region formed through the potential differences in the device structure. In this sense, the diffusion component can be excluded due to the large built-in field additionally created in QD layers so that photogenerated electrons in the QD layers, regardless of the position, are swept quickly by the electric field as a drift current to the MoS_2 channel. The resulting rise and decay times of the double-junction device are plotted to show the outstanding response time in Figure 3b left, with a rise time of 950 μs and a decay time of 1 ms for 850 nm laser excitation.

The fast response time observed for the hybrid-structured device, when subjected to laser illumination at a wavelength of 850 nm, can be attributed not only to the internal electric field within the QD layers, but also to the laser excitation energy being less than the band gap of the MoS_2 monolayer (~1.88 eV). For a pristine MoS_2 monolayer, oxygen/water adsorbates[30,31] are generally responsible for the slow photoresponse time (1−100 s) when the photon energy exceeds the electronic band gap of the MoS_2 monolayer, as previously reported for MoS_2 photodetectors.[14,30] This behavior is also observed in our pristine MoS_2 and MoS_2/PbS QDs devices when a 532 nm ($>E_{g,MoS_2}$) laser was used as the illumination source (Figure 3b, middle and right). Even though the photoresponse time is decreased for the MoS_2/PbS QDs device compared to the pristine MoS_2 device under 532 nm laser excitation, there still remains a noticeable decay tail after the laser source is switched off. This implies that the dominant trap-assisted photoresponse of the MoS_2 layer can still be observed even in the hybrid-structured device. Therefore, for the optimum detector performance, the roles of the charge-transporting layer and the light-absorbing medium should be decoupled.

Phototransistor Performance. The results presented thus far demonstrate the benefits of the presence of an internal electric field within the light-absorbing layers. We now consider the phototransistor performance of the double-junction device. The presence of a back-gate in the phototransistor structure can be used to modulate the conductivity of the MoS_2 channel as well as the overall optoelectronic performance of the device. In this hybrid-structured device, the Fermi level (E_F) of MoS_2 is modulated through electrical gating. In this case, the effective Schottky barriers at the source and drain electrodes are lowered for positive back-gate voltages (accumulation regime) and increased when negative polarity back-gate voltages are applied (depletion regime); this, in turn, affects the dark level and charge transport that governs the sensitivity of the detector. Figure 4a shows the calculated photoresponsivity of the hybrid-structured device under various illumination intensities and gate voltages. A clear trend showing an increase in the photoresponsivity is observed as the amplitude of the positive gate voltage was increased, with the maximum photoresponsivity reaching $R = 5.4 \times 10^4$ A/W. This can be explained as follows: when illuminated with 850 nm laser light, the photogenerated electrons are transferred from the QD layers to the MoS_2 monolayer. For positive polarity back-gate voltages, the Schottky barrier height between the MoS_2 channel and the source−drain electrodes is lowered,[32,33] and charges can then effectively propagate into the MoS_2 layer, resulting in higher photoconductive gain in the detector. On the other hand, the transport of charges is hampered when the Schottky barrier height is increased.

To evaluate the sensitivity of the double-junction device, the signal-to-noise ratio (SNR) and detectivity were measured for different gate voltages, as shown in Figure 4b. The SNR was measured under an incident laser power of 200 nW. The detectivity D^*[1,20] at 1 Hz bandwidth is defined as $D^* = \frac{\sqrt{AB}}{\mathrm{NEP}}$ in unit of jones (1 jones = 1 cm $\mathrm{Hz}^{1/2}$/W), where A is the active area of the device, B is the noise bandwidth, and NEP (NEP = i_n/R) is the noise-equivalent power, which is the minimum detectable power when the signal-to-noise ratio is

DOI: 10.1021/acsami.8b14408
ACS Appl. Mater. Interfaces 2018, 10, 38264−38271

equal to unity. Whereas the photoresponsivity is decreased when negative polarity gate voltages are applied, the sensitivity of the detector is largely increased, with the maximum detectivity reaching around $D^* = 1 \times 10^{11}$ jones. The improvement in the sensitivity for the negative polarity voltage regime can be attributed to the significantly reduced dark level and increased SNR. Thus, with a semiconducting MoS_2 channel in a 2D/QD hybrid-structured phototransistor, where a modulation of the gate-field is possible, the sensitivity can be enhanced by operating the device in the depletion regime. The key figures of merit of phototransistors are compared in Table S1. For the first time, we employed CVD-grown monolayered MoS_2 and consecutive QD junction structures into the phototransistor, which resulted in the outstanding performance in terms of the response time, photoresponsivity, and directivity compared to earlier studies on MoS_2 and equivalent hybrid structures.

CONCLUSIONS

In conclusion, we have demonstrated an evident enhancement in the optoelectronic performance in a MoS_2/PbS QDs hybrid-structured phototransistor when a large built-in potential is created within the QD layers. The effects of the built-in potential were clearly observed through the enhancement of the photoresponsivity and photoresponse times, which were found to reach values of 5.4×10^4 A/W and 950 μs, respectively; we have attributed the improvement to the efficient separation of excitons and transfer of charges in a preferred direction toward the channel. In particular, the response time observed in this work is orders of magnitude shorter than that observed in previously reported 2D/QD phototransistors. We have also demonstrated a gate-field modulation of the phototransistor so that the device can be operated in the depletion mode with values for the detectivity up to $D^* = 1 \times 10^{11}$ jones. The efficient charge transfer in the MoS_2/QDs architecture through the employment of QD junctions, demonstrated herein, presents an important strategy in the design of photodetectors based on 2D/0D and other mixed-dimensional van der Waals hybrid structures.

MATERIALS AND METHODS

CVD Synthesis of MoS_2 Monolayer. A MoS_2 monolayer was grown on a SiO_2 (300 nm)/Si substrate using a chemical vapor deposition method. To summarize, the synthesis was carried out inside a 2 in. furnace tube. A 0.1 mg of MoO_3 powders was loaded onto an alumina boat with the substrate facing down the boat. Another boat containing 50 mg of sulfur powders was placed upstream of the furnace. CVD growth was carried at 750 °C for 10 min, with an Ar gas flow of 150 sccm. The furnace was then allowed to cool down to room temperature.

Colloidal PbS QD Synthesis. PbS CQDs with an absorption peak at 953 nm (1.30 eV) were synthesized using a method that we have described elsewhere.[34,35] A Pb precursor solution was prepared by mixing lead oxide (PbO), oleic acid, and 1-octadecene (ODE) in a 50 mL two-neck flask. The solution was heated to 100 °C under vacuum for 3 h before the heating temperature was elevated to 130 °C for further treatment of the precursor solution under an argon (Ar) environment for 1 h. A sulfur precursor solution was produced by mixing hexamethyldisilathiane and ODE in a 50 mL two-neck flask and then treated for 4 h at room temperature in an Ar environment. The PbS CQD synthesis was proceeded by rapid injection of the sulfur precursor solution into the Pb precursor solution. The purification and washing steps were applied to the PbS CQDs solution and then PbS CQDs were finally dispersed in a toluene solvent at a concentration of 50 mg/mL.

Device Fabrication and Measurement. To fabricate the MoS_2 device, electrode contacts were drawn by a standard electron beam lithography process (Raith e-LiNE Plus), followed by the sequential deposition of titanium (5 nm) and gold (45 nm) using a thermal deposition process. The fabricated devices have an active device area of 200 μm^2, with a channel length of 5 μm and channel width of 40 μm. To fabricate the MoS_2/PbS hybrid-structured device, the PbS colloidal QD solution was spin-coated six times by layer by layer so as to deposit the QDs onto the MoS_2 device at a spin rate of 3000 rpm. Six layers of the TBAI ligand-exchanged PbS QDs and four layers of the TBAI ligand-exchanged PbS QDs with two layers of the EDT ligand-exchanged PbS QDs were deposited for the fabrication of the MoS_2/TBAI and MoS_2/TBAI/EDT devices, respectively. For a solid-state ligand-exchange process, a tetrabutylammonium iodide (TBAI) solution in methanol at a concentration of 10 mg/mL was applied to a PbS QD layer for 30 s. A TBAI-treated CQD layer was then rinsed twice using methanol. Similarly, 1,2-ethanedithiol (EDT) at a concentration of 0.02 v/v% in acetonitrile was applied to a PbS CQD layer that was deposited onto the TBAI-treated CQD layer. After 30 s of EDT treatment, the EDT-treated CQD layer was washed using acetonitrile, twice. The spin-coating speed was fixed at 3000 rpm for the whole process. The (opto)electronic properties of the fabricated MoS_2 and MoS_2/PbS QDs devices were measured using the semiconductor characterization system (4200-SCS, Keithley), Lecroy HD4000 high-definition oscilloscope, Stanford Research Systems SR570 current preamplifier, and Cascade Microtech probe station.

ASSOCIATED CONTENT

Supporting Information

The Supporting Information is available free of charge on the ACS Publications website at DOI: 10.1021/acsami.8b14408.

Raman, PL, and TEM analysis of MoS_2, AFM height profile of PbS QDs, absorption spectra, X-ray diffraction spectra, and HRTEM image of PbS QDs, Fourier transform infrared spectroscopy analysis of the ligand-exchanged PbS QDs, UPS measurements of PbS QDs with the TBAI and EDT ligands, photoresponsivity measurements respective to the incident laser powers, and performance of photodetectors (PDF)

AUTHOR INFORMATION

Corresponding Authors

*E-mail: junginn.sohn@dongguk.edu (J.I.S.).
*E-mail: chasn@skku.edu, seungnam.cha@eng.ox.ac.uk. Tel: +44-1865-273010. Fax: +44-1865-273912 (S.N.C.).

ORCID

Sangyeon Pak: 0000-0003-1765-3043
Yuljae Cho: 0000-0003-2976-0604
John Hong: 0000-0002-1513-8622
Bo Hou: 0000-0001-9918-8223
Young-Woo Lee: 0000-0003-0777-8221
Jae Eun Jang: 0000-0002-8523-1785
Jung Inn Sohn: 0000-0002-3155-4327
SeungNam Cha: 0000-0001-6284-8312

Author Contributions

$^{\nabla}$S.P. and Y.C. contributed equally to this work.

Notes

The authors declare no competing financial interest.

ACKNOWLEDGMENTS

The research leading to these results has received funding from the European Research Council under the European Union's

DOI: 10.1021/acsami.8b14408
ACS Appl. Mater. Interfaces 2018, 10, 38264−38271

Seventh Framework Programme (FP/2007−2013)/ERC Grant Agreement no. 340538. This work was also supported by the National Research Foundation of Korea (NRF) (2015M2A2A6A02045252) and Samsung Global Research Outreach (Samsung GRO) program. In addition, S.M.M. would like to thank The Royal Society for financial support.

REFERENCES

(1) Konstantatos, G.; Sargent, E. H. Nanostructured Materials for Photon Detection. *Nat. Nanotechnol.* **2010**, *5*, 391−400.
(2) Novoselov, K. S.; Mishchenko, A.; Carvalho, A.; Neto, C. A. H. 2d Materials and Van Der Waals Heterostructures. *Science* **2016**, *353*, No. aac9439.
(3) Buscema, M.; Island, J. O.; Groenendijk, D. J.; Blanter, S. I.; Steele, G. A.; van der Zant, H. S. J.; Castellanos-Gomez, A. Photocurrent Generation with Two-Dimensional Van Der Waals Semiconductors. *Chem. Soc. Rev.* **2015**, *44*, 3691−3718.
(4) Pak, S.; Lee, J.; Lee, Y.-W.; Jang, A.-R.; Ahn, S.; Ma, K. Y.; Cho, Y.; Hong, J.; Lee, S.; Jeong, H. Y.; Im, H.; Shin, H. S.; Morris, S. M.; Cha, S.; Sohn, J. I.; Kim, J. M. Strain-Mediated Interlayer Coupling Effects on the Excitonic Behaviors in an Epitaxially Grown MoS2/WS2 Van Der Waals Heterobilayer. *Nano Lett.* **2017**, *17*, 5634−5640.
(5) McDonald, S. A.; Konstantatos, G.; Zhang, S.; Cyr, P. W.; Klem, E. J.; Levina, L.; Sargent, E. H. Solution-Processed PbS Quantum Dot Infrared Photodetectors and Photovoltaics. *Nat. Mater.* **2005**, *4*, 138−142.
(6) Kim, B.-S.; Neo, D. C. J.; Hou, B.; Park, J.; Cho, Y.; Zhang, N.; Hong, J.; Pak, S.; Lee, S.; Sohn, J.; Assender, H. E.; Watt, A. A. R.; Cha, S.; Kim, J. High Performance PbS Quantum Dot/Graphene Hybrid Solar Cell with Efficient Charge Extraction. *ACS Appl. Mater. Interfaces* **2016**, *8*, 13902−13908.
(7) Hong, J.; Hou, B.; Lim, J.; Pak, S.; Kim, B. S.; Cho, Y.; Lee, J.; Lee, Y.-W.; Giraud, P.; Lee, S.; Park, J. B.; Morris, S. M.; Snaith, H. J.; Sohn, J. I.; Cha, S.; Kim, J. M. Enhanced Charge Carrier Transport Properties in Colloidal Quantum Dot Solar Cells Via Organic and Inorganic Hybrid Surface Passivation. *J. Mater. Chem. A* **2016**, *4*, 18769−18775.
(8) Cho, Y.; Giraud, P.; Hou, B.; Lee, Y.-W.; Hong, J.; Lee, S.; Pak, S.; Lee, J.; Jang, J. E.; Morris, S. M.; Sohn, J. I.; Cha, S.; Kim, J. M. Charge Transport Modulation of a Flexible Quantum Dot Solar Cell Using a Piezoelectric Effect. *Adv. Energy Mater.* **2018**, *8*, No. 1700809.
(9) Cho, Y.; Lee, S.; Hong, J.; Pak, S.; Hou, B.; Lee, Y. W.; Jang, J. E.; Im, H.; Sohn, J. I.; Cha, S.; Kim, J. M. Sustainable Hybrid Energy Harvester Based on Air Stable Quantum Dot Solar Cells and Triboelectric Nanogenerator. *J. Mater. Chem. A* **2018**, *6*, 12440−12446.
(10) Giraud, P.; Hou, B.; Pak, S.; Sohn, J. I.; Morris, S.; Cha, S.; Kim, J. M. Field Effect Transistors and Phototransistors Based Upon P-Type Solution-Processed PbS Nanowires. *Nanotechnology* **2018**, *29*, No. 075202.
(11) Sohn, J. I.; Hong, W. K.; Lee, M. J.; Lee, T.; Sirringhaus, H.; Kang, D. J.; Welland, M. E. The Influence of Surface Chemical Dynamics on Electrical and Optical Properties of ZnO Nanowire Field Effect Transistors. *Nanotechnology* **2009**, *20*, No. 505202.
(12) Wang, Q. H.; Kalantar-Zadeh, K.; Kis, A.; Coleman, J. N.; Strano, M. S. Electronics and Optoelectronics of Two-Dimensional Transition Metal Dichalcogenides. *Nat. Nanotechnol.* **2012**, *7*, 699−712.
(13) Lee, J.; Pak, S.; Giraud, P.; Lee, Y.-W.; Cho, Y.; Hong, J.; Jang, A.-R.; Chung, H. S.; Hong, W.-K.; Jeong, H. Y.; Shin, H. S.; Occhipinti, L. G.; Morris, S. M.; Cha, S.; Sohn, J. I.; Kim, J. M. Thermodynamically Stable Synthesis of Large-Scale and Highly Crystalline Transition Metal Dichalcogenide Monolayers and Their Unipolar n-n Heterojunction Devices. *Adv. Mater.* **2017**, *29*, No. 1702206.
(14) Lee, J.; Pak, S.; Lee, Y.-W.; Cho, Y.; Hong, J.; Giraud, P.; Shin, H. S.; Morris, S. M.; Sohn, J. I.; Cha, S.; Kim, J. M. Monolayer Optical Memory Cells Based on Artificial Trap-Mediated Charge Storage and Release. *Nat. Commun.* **2017**, *8*, No. 14734.
(15) Konstantatos, G.; Badioli, M.; Gaudreau, L.; Osmond, J.; Bernechea, M.; de Arquer, G. F. P.; Gatti, F.; Koppens, F. H. Hybrid Graphene-Quantum Dot Phototransistors with Ultrahigh Gain. *Nat. Nanotechnol.* **2012**, *7*, 363−368.
(16) Chen, X.; Liu, X.; Wu, B.; Nan, H.; Guo, H.; Ni, Z.; Wang, F.; Wang, X.; Shi, Y.; Wang, X. Improving the Performance of Graphene Phototransistors Using a Heterostructure as the Light-Absorbing Layer. *Nano Lett.* **2017**, *17*, 6391−6396.
(17) Kufer, D.; Konstantatos, G. Photo-Fets: Phototransistors Enabled by 2D and 0D Nanomaterials. *ACS Photonics* **2016**, *3*, 2197−2210.
(18) Kufer, D.; Lasanta, T.; Bernechea, M.; Koppens, F. H. L.; Konstantatos, G. Interface Engineering in Hybrid Quantum Dot−2D Phototransistors. *ACS Photonics* **2016**, *3*, 1324−1330.
(19) Nikitskiy, I.; Goossens, S.; Kufer, D.; Lasanta, T.; Navickaite, G.; Koppens, F. H.; Konstantatos, G. Integrating an Electrically Active Colloidal Quantum Dot Photodiode with a Graphene Phototransistor. *Nat. Commun.* **2016**, *7*, No. 11954.
(20) Kufer, D.; Nikitskiy, I.; Lasanta, T.; Navickaite, G.; Koppens, F. H.; Konstantatos, G. Hybrid 2d-0d MoS2 -PbS Quantum Dot Photodetectors. *Adv. Mater.* **2015**, *27*, 176−180.
(21) Huo, N.; Gupta, S.; Konstantatos, G. MoS2 -HgTe Quantum Dot Hybrid Photodetectors Beyond 2 μm. *Adv. Mater.* **2017**, *29*, No. 1606576.
(22) Chuang, C.-H. M.; Brown, P. R.; Bulović, V.; Bawendi, M. G. Improved Performance and Stability in Quantum Dot Solar Cells through Band Alignment Engineering. *Nat. Mater.* **2014**, *13*, 796−801.
(23) Rekemeyer, P. H.; Chuang, C.-H. M.; Bawendi, M. G.; Gradečak, S. Minority Carrier Transport in Lead Sulfide Quantum Dot Photovoltaics. *Nano Lett.* **2017**, *17*, 6221−6227.
(24) Barkhouse, D. A. R.; Debnath, R.; Kramer, I. J.; Zhitomirsky, D.; Pattantyus-Abraham, A. G.; Levina, L.; Etgar, L.; Grätzel, M.; Sargent, E. H. Depleted Bulk Heterojunction Colloidal Quantum Dot Photovoltaics. *Adv. Mater.* **2011**, *23*, 3134−3138.
(25) Choi, J. J.; Luria, J.; Hyun, B. R.; Bartnik, A. C.; Sun, L.; Lim, Y. F.; Marohn, J. A.; Wise, F. W.; Hanrath, T. Photogenerated Exciton Dissociation in Highly Coupled Lead Salt Nanocrystal Assemblies. *Nano Lett.* **2010**, *10*, 1805−1811.
(26) Burke, T. M.; Sweetnam, S.; Vandewal, K.; McGehee, M. D. Beyond Langevin Recombination: How Equilibrium between Free Carriers and Charge Transfer States Determines the Open-Circuit Voltage of Organic Solar Cells. *Adv. Energy Mater.* **2015**, *5*, No. 1500123.
(27) Ren, Z.; Sun, J.; Li, H.; Mao, P.; Wei, Y.; Zhong, X.; Hu, J.; Yang, S.; Wang, J. Bilayer PbS Quantum Dots for High-Performance Photodetectors. *Adv. Mater.* **2017**, *29*, No. 1702055.
(28) Clifford, J. P.; Konstantatos, G.; Johnston, K. W.; Hoogland, S.; Levina, L.; Sargent, E. H. Fast, Sensitive and Spectrally Tuneable Colloidal-Quantum-Dot Photodetectors. *Nat. Nanotechnol.* **2009**, *4*, 40−44.
(29) Yu, Y.; Zhang, Y. T.; Song, X. X.; Zhang, H. T.; Cao, M. X.; Che, Y. L.; Dai, H. T.; Yang, J. B.; Zhang, H.; Yao, J. Q. Pbs-Decorated WS2 Phototransistors with Fast Response. *ACS Photonics* **2017**, *4*, 950−956.
(30) Zhang, W.; Huang, J.-K.; Chen, C.-H.; Chang, Y.-H.; Cheng, Y.-J.; Li, L.-J. High-Gain Phototransistors Based on a CVD MoS2 Monolayer. *Adv. Mater.* **2013**, *25*, 3456−3461.
(31) Wu, Y.-C.; Liu, C.-H.; Chen, S.-Y.; Shih, F.-Y.; Ho, P.-H.; Chen, C.-W.; Liang, C.-T.; Wang, W.-H. Extrinsic Origin of Persistent Photoconductivity in Monolayer MoS2 Field Effect Transistors. *Sci. Rep.* **2015**, *5*, No. 11472.
(32) Zhang, W.; Chiu, M. H.; Chen, C. H.; Chen, W.; Li, L. J.; Wee, A. T. S. Role of Metal Contacts in High-Performance Phototransistors Based on WSe2 Monolayers. *ACS Nano* **2014**, *8*, 8653−8661.
(33) Yu, Y.; Zhang, Y.; Zhang, Z.; Zhang, H.; Song, X.; Cao, M.; Che, Y.; Dai, H.; Yang, J.; Wang, J.; Zhang, H.; Yao, J. Broadband

DOI: 10.1021/acsami.8b14408
ACS Appl. Mater. Interfaces 2018, 10, 38264−38271

Phototransistor Based on CH3NH3PBI3 Perovskite and PbSe Quantum Dot Heterojunction. *J. Phys. Chem. Lett.* **2017**, *8*, 445−451.
(34) Hou, B.; Cho, Y.; Kim, B. S.; Hong, J.; Park, J. B.; Ahn, S. J.; Sohn, J. I.; Cha, S.; Kim, J. M. Highly Monodispersed PbS Quantum Dots for Outstanding Cascaded-Junction Solar Cells. *ACS Energy Lett.* **2016**, *1*, 834−839.
(35) Cho, Y.; Hou, B.; Lim, J.; Lee, S.; Pak, S.; Hong, J.; Giraud, P.; Jang, A. R.; Lee, Y. W.; Lee, J.; Jang, J. E.; Snaith, H. J.; Morris, S. M.; Sohn, J. I.; Cha, S.; Kim, J. M. Balancing Charge Carrier Transport in a Quantum Dot P-N Junction toward Hysteresis-Free High-Performance Solar Cells. *ACS Energy Lett.* **2018**, *3*, 1036−1043.

DOI: 10.1021/acsami.8b14408
ACS Appl. Mater. Interfaces 2018, 10, 38264−38271